Degradation intermediates and reaction pathway of pyraclostrobin with TiO$_2$ photocatalysis

Laura Lagunas-Allué [a,c,*], María-Teresa Martínez-Soria [a], Jesús Sanz-Asensio [a], Arnaud Salvador [b], Corinne Ferronato [c], Jean Marc Chovelon [c]

[a] Department of Chemistry, University of La Rioja, Madre de Dios, 51, 26006 Logroño, Spain
[b] Laboratoire des sciences Analytiques, UMR 5180, Batiment CPE, 43, Boulevard du 11 novembre 1918, Université de Lyon, 69622 Villeurbanne cedex, France
[c] Université Lyon 1, CNRS, UMR 5256, IRCELYON, Institut de recherches sur la catalyse et l'environnement de Lyon, 2 avenue Albert Einstein, F-69626 Villeurbanne, France

ARTICLE INFO

ABSTRACT

The present study deals with the photocatalytic degradation of the strobilurin pyraclostrobin in the presence of titanium dioxide (TiO$_2$) as a photocatalyst and UV light irradiation. The obtained results show a complete degradation of pyraclostrobin at pH 6.2, temperature at $20 \pm 1\,^{\circ}$C and $0.5\,g\,L^{-1}$ of catalyst after 60 min irradiation. Photodegradation of pyraclostrobin exhibited pseudo-first-order reaction kinetics. The rate of photodecomposition of pyraclostrobin was measured using high performance liquid chromatography–diode array detector (HPLC–DAD). The effect of solution pH in the 2–10 range was investigated as well as the reaction intermediates formed during degradation. To obtain a better understanding of the mechanistic details of this TiO$_2$-assisted photodegradation of pyraclostrobin with UV-irradiation, the intermediates of the processes were concentrated, separated and identified by the solid-phase extraction (SPE) and liquid chromatography/mass spectrometry (LC–MS/MS) technique. The probable photodegradation pathways were proposed and discussed. The main steps involved: hydroxylation of the aromatic rings (chloro-phenyl, phenyl and pyrazol) followed by the loss of the N-methoxy group, substitution of chloride atom by a hydroxyl group, rupture of the pyrazol and phenyl bond and the scission of the oxygen and pyrazol bond.

1. Introduction

In recent years, heterogeneous photocatalysis for total oxidation of many pesticides, herbicides, surfactants and colorings has been studied extensively [1–5]. This technique is based on the use of UV irradiated semiconductors, generally titanium dioxide creating a redox environment which is able to destroy these pollutants oxidizing them into mineralized products like carbon dioxide, water and eventually inorganic ions such as chloride, nitrate, ammonium and sulfate.

Basically, the photodegradation via TiO$_2$ is initiated by the generation of hole/electron pairs (h$^+$/e$^-$) in the semiconductor valence (h$_{VB}^+$) and conduction bands (e$_{CB}^-$), respectively, upon absorption of ultra-violet (UV) light with energy equal to or higher than the corresponding band gap energy (>3.2 eV for TiO$_2$ anatase) as shown as follows:

$$TiO_2 + h\nu \rightarrow h_{VB}^+ + e_{CB}^-$$
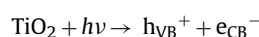
The charges carriers, h_{VB}^+ and e_{CB}^-, can recombine, or h_{VB}^+ can be scavenged by oxidizing species (for example, H$_2$O, OH$^-$, organic compound), and e_{CB}^- by reducing species (for example, O$_2$) in the solution leading mainly to the formation of hydroxyl radicals (OH$^•$) as well as superoxide radical anions (O$_2^{•-}$) and hydroperoxyl radicals (HOO$^•$) on the surface of TiO$_2$, which are able to destroy a large variety of toxic organic compounds [6–9].

In this study, photocatalytic degradation of pyraclostrobin was carried out by TiO$_2$ in aqueous solution. Pyraclostrobin is a completely new active ingredient belonging to the strobilurins group of fungicides. This group of fungicides acts through inhibition of mitochondrial respiration by blocking electron transfer within the respiratory chain, which in turn causes important cellular biochemical processes to be severely disrupted, and results in cessation of fungal growth. Pyraclostrobin is recommended for the prevention and treatment of powdery mildew and downy mildew in fruit plants and vines. This pesticide is moderately toxic for bees and extremely toxic for fish. Besides it, pyraclostrobin has been previously found in analysis of surface and groundwater samples [10], therefore it is important to use treatment methods for the removal of this pollutant from water.

The aim of this paper is to assess the effectiveness of the photocatalytic process for the decontamination of water polluted by

* Corresponding author.
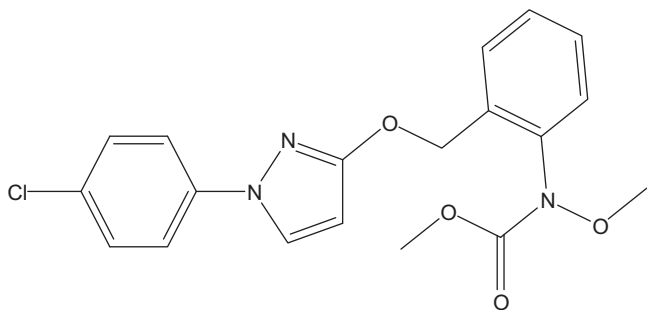E-mail address: laura.lagunas@unirioja.es (L. Lagunas-Allué).

Fig. 1. Chemical structure of pyraclostrobin.

pyraclostrobin, to evaluate the kinetics aspects of the process (adsorption, degradation rate, photolysis, etc.) and the identification of the reaction intermediates for understanding the mechanistic details of the photodegradation in the TiO_2/UV light process.

2. Experimental

2.1. Materials and reagents

Pyraclostrobin [methyl N-{2-[1-(4-chlorophenyl)-1H-pyrazol-3-yloxymethyl] phenyl}(N-methoxy) carbamate] (Fig. 1) purity >99% was purchased from Riedel-de-Haën (Seelze, Germany). It was used without further purification.

The solvents used for HPLC analyses were methanol and acetonitrile HPLC grade from SDS Carlo Erba (Peypin, France). Formic acid (MS grade, 99% purity) was from Aldrich. All the solutions were prepared with ultra pure water obtained with a Millipore-Milli Q system. Other reagents were at least of analytical grade.

All the irradiated solutions were prepared from a pyraclostrobin solution containing $2.3\,mg\,L^{-1}$ or $5.9\,\mu mol\,L^{-1}$ and stored at $4\,°C$. Non-porous titanium dioxide (TiO_2, P25, Degussa AG, Germany) with primary particle diameter of 30 nm and specific surface area of ca. $50\,m^2\,g^{-1}$ was used as the photocatalyst.

Polyvinylidene fluoride (PVDF) filters (0.45 nm) were purchased from Millipore (Molsheim, France).

2.2. Photoreactor and light source

The irradiation experiments were performed using a high pressure mercury UV lamp (PHILIPS HPK 125 W) emitting in the near-UV (mainly around 365 nm) and equipped with an open Pyrex glass cell of ca. 60 mL containing the aqueous suspension magnetically stirred of pyraclostrobin and TiO_2 powder ($0.5\,g\,L^{-1}$). The photoreactor was cooled with a water circulation for carrying out the experiments at $20\,°C$ and filtered with a 340 nm cut-off filter made of Pyrex. The light flux entering the reactor was measured directly using a radiometer (Bioblock, Illkirch, France Scientific model CX-365).

2.3. Procedure

A volume of 25 mL of a solution of pyraclostrobin ($2.3\,mg\,L^{-1}$) and 12.5 mg of TiO_2 were put into the reactor and vigorously stirred. The solution was allowed to stay in the dark during 15 min to reach adsorption equilibrium and then, it was irradiated. During kinetic experiments, 300 μL aliquots were sampled during adsorption and at different irradiation times and filtered through 0.45 μm PVDF Millipore filters to remove TiO_2 particles before analyses.

All the experiments were performed at a natural pH ≈ 6.2, with the reactor opened to the air and the temperature was initially fixed at $20 ± 1\,°C$ and controlled throughout the experiment.

2.4. Solid-phase extraction

Before separating and identifying the intermediates formed during the pyraclostrobin degradation, the irradiated suspensions were concentrated by the solid-phase extraction (SPE) method. A sample volume of 25 mL was passed through the Isolute C_{18} cartridges 500 mg/6 mL (International Sorbent Technology, Cambridge, UK), previously conditioned with 6 mL of methanol followed by 6 mL of water using a Varian vacuum manifold. Then, the retained compounds were eluted with two aliquots of 0.5 mL methanol.

2.5. Analytical determination

2.5.1. HPLC–UV and HPLC–DAD analyses

The evolution of pyraclostrobin concentration was monitored by HPLC using a Shimadzu LC-10AT binary pump system equipped with a SPD-M10A DAD and fitted with a reverse phase YP5 B C_{18} (125 mm × 4 mm, 5 μm) and a pre-column. Detection of pyraclostrobin was carried out at 275 nm. The isocratic elution conditions were methanol/water (65:35, v/v). It was eluted with a rate of $1.0\,mL\,min^{-1}$ and the injection volume was 20 μL. Carboxylic acids were identified and quantified by ion-exclusion chromatography using the HPLC-UV system (Varian 9010 model) equipped with a COREGEL 87-H3 cation exchange column (300 mm × 7.8 mm, 9 μm). The mobile phase was H_2SO_4 (pH ≈ 2.0) at a flow rate of $0.6\,mL\,min^{-1}$. The injection volume was 100 μL. The wavelength for detection was 210 nm.

2.5.2. HPLC–MS/MS analysis

The identification of intermediates was performed by HPLC–MS/MS. In order to detect and identify the maximum number of degradation products, a SPE concentration of 25 mL irradiated solution was performed. Then, a 20 μL sample was injected. LC–MS analyses were performed on a system consisting of an HP 1100 series HPLC instrument comprising a binary pump and autosampler (Agilent Technologies, Waldbronn, Germany) coupled to a API3000 triple quadrupole mass spectrometer (Applied Biosystems/MDS Analytical Technologies, Foster City, CA, USA) equipped with a Heated Nebulizer source (APCI). The LC separation was carried out on a Prontosil C_{18} column, (125 mm × 2 mm, 3 μm) from Atlantic Labo I.C.S. (Bruges, France). Elution was performed at a flow rate of $300\,\mu L\,min^{-1}$ with water containing 0.1% (v/v) formic acid as eluent A and acetonitrile containing 0.1% (v/v) formic acid as eluent B, employing a linear gradient from 10% B to 100% B in 25 min. MS analysis was carried out mainly in positive ionization mode using a nebulizer current of 4 A. Instrument control, data acquisition and processing were performed using the associated Analyst 1.4.2 software. The mass spectrometer was initially calibrated using polypropylene glycol (Applied Biosystems, Foster City, CA, USA). Q1 and Q3 were adjusted to $0.7 ± 0.1$ a.m.u. FWHM for Full Scan, Product Ion scan and single ion monitoring mode, referred to as unit resolution. The nebulizer (air) and the curtain gas flows (nitrogen) were respectively set at 12 and 10 arbitrary unit (AU). The APCI source was operated at $500\,°C$ with the auxiliary gas flow (air) set at $8\,L\,min^{-1}$.

Kinetic photo-degradation determinations were performed in single ion monitoring (SIM) (Declustering potential 26 V, Focussing potential 170 V, Entrance potential, 10 V). Structural information was obtained with information dependent acquisition (IDA) enables automated MS to MS/MS acquisition with collision energy at 20 and 40 eV.
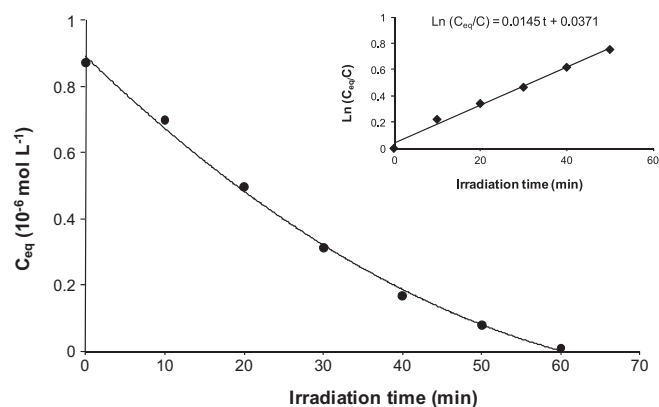
Fig. 2. Photocatalytic degradation of pyraclostrobin (5.9 μmol L^{-1}). The inset shows the linear transform of the integrated first-order kinetics.

In order to better understand the reaction mechanisms involved in the photocatalytic degradation of pyraclostrobin, the kinetic evolution of principal intermediates was also followed during the irradiation of a solution of pyraclostrobin (2.3 mg L^{-1}) under a photonic flux of 4.6×10^{15} photon s^{-1} cm^{-2}. Thus, aliquots (300 μL) of the reaction mixture were sampled at the beginning of the experiment and at regular time intervals (10 or 15 min) during photodegradation process up to 300 min (after filtration to separate the TiO$_2$ particles) and analyzed by HPLC–MS/MS. After 150 min of irradiation, degradation products were not detected.

2.6. Computer simulations

The optimal geometry of the ground state of the pyraclostrobin molecule was obtained by DFT quantum calculations performed at B3LYP/6-31g level. The atomic charges on the molecule were obtained by fitting to the electrostatic potential according to the Merz–Singh–Kollman scheme [11]. These calculations were carried out using Gaussian 09 software [12].

3. Results and discussion

3.1. Kinetics of pyraclostrobin degradation

Several experimental studies have indicated that the photocatalytical degradation rates of pesticides over illuminated TiO$_2$ could be interpreted by the Langmuir–Hinshelwood (L–H) kinetic model [13–15]. The photocatalytic degradation of 5.9 μmol L^{-1} pyraclostrobin is presented in Fig. 2 while, in the inset, the logarithm of the ratio of the initial concentration (C_{eq}) to the concentration at a given time (C) versus time (t) is plotted. The degradation fitted

Table 1
The pseudo first-order rate constant k_{obs}, half-life $t_{1/2}$, and correlation coefficients for photocatalytic degradation of pyraclostrobin at different pH.

pH	k_{obs} (10^{-2} min^{-1})	$t_{1/2}$ (min)	r^2
10.0	0.54	128.4	0.9681
7.9	0.63	110.0	0.9807
Natural	1.45	47.8	0.9913
4.1	1.56	44.4	0.9939
2.0	1.80	38.5	0.9942

well the exponential decay curve, following first-order behavior consistent to the Langmuir–Hinshelwood model. The rate constant (k_{obs}) was determined by calculating the slope of the line obtained (1.4×10^{-2} min^{-1}). About 99% of the pyraclostrobin was degraded after UV irradiation for 60 min.

The photolysis (blank experiment without photocatalyst) of the tested pesticide followed also first-order kinetic. The value of the photolysis rate constant (k_{phot}) obtained was 0.9×10^{-3} min^{-1}. As it can be observed from these rate constants, the contribution of the direct photolysis in the photodegradation was low for pyraclostrobin. The photocatalysis process was demonstrated to be around 15 times faster than direct photolysis.

3.2. Effect of pH

In this study, the initial pH was maintained at 2.0, 4.1, 7.9 or 10.0 in a suspension of 0.5 g L^{-1} TiO$_2$ and 2.3 mg L^{-1} pyraclostrobin. Whatever the pH values studied, the disappearance of pyraclostrobin obeyed an apparent first-order kinetic. The kinetic rate constant values for the degradation of pyraclostrobin as a function of reaction pH are summarized in Table 1. As reported, the pH of the suspension appeared to have little effect on the rate of disappearance of pyraclostrobin between pH 2.0 and pH 6.2 and gradually decreases upon increasing the pH from pH 7.0 to pH 10.0.

The ionization state of the surface the photocatalyst can be protonated and deprotonated under acidic and alkaline conditions, respectively, as shown in following equations:

$$TiOH + H^+ \leftrightarrow TiOH_2^+ \qquad (1)$$

$$TiOH + OH^- \leftrightarrow TiO^- + H_2O \qquad (2)$$

The point of zero charge (pzc) of the TiO$_2$ (Degussa P25) is widely reported at pH ~6.25 [16]. This means that the TiO$_2$ surface is positively charged when the pH is lower than this value and negatively charged above. Therefore, pH value will have a significant effect on the adsorption/desorption properties at the catalyst's surface [17].

Different charge densities may be generated in the pyraclostrobin molecule depending on the type of interaction with the titanium dioxide surface, accelerating or retarding the degradation.
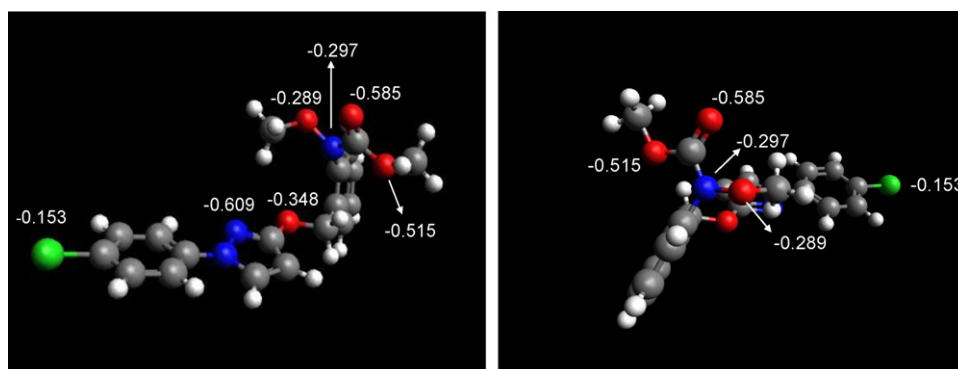

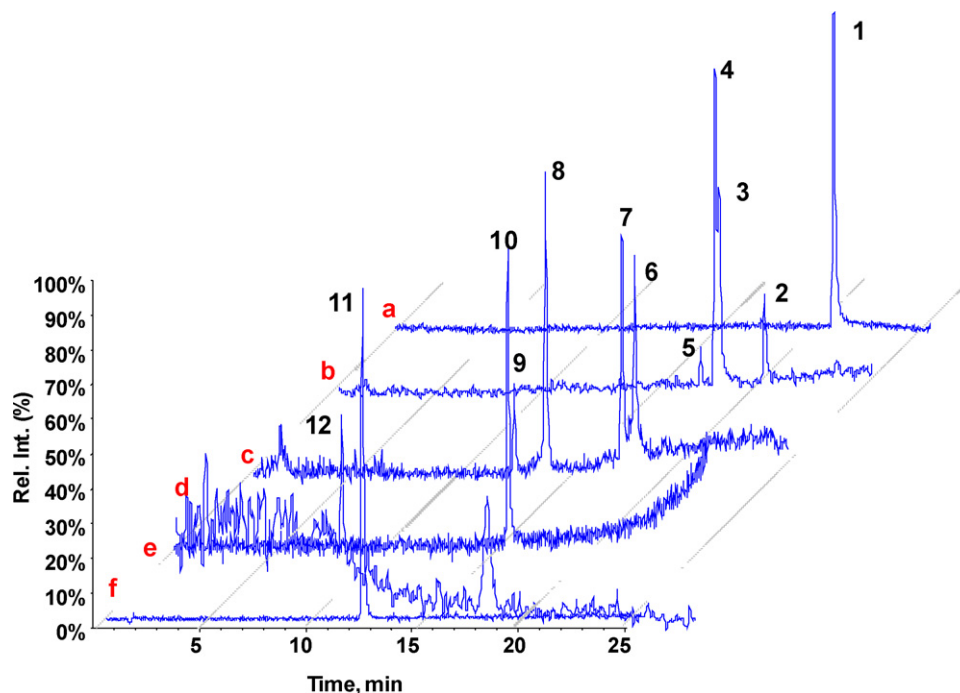**Fig. 3.** Charge densities on some atoms in pyraclostrobin.

Fig. 4. Positive APCI–LC–MS/MS chromatograms of pyraclostrobin degradation mixtures (a) single ion monitoring (SIM) $m/z = 388$ of pyraclostrobin, (b) SIM of monohydroxylated pyraclostrobin $m/z = 404$, (c) SIM of hydroxylated pyraclostrobin with loss of the N-methoxy group $m/z = 374$, (d) SIM of $m/z = 370$, (e) SIM of $m/z = 212$ (f) SIM of $m/z = 278$ (see Table 2 and Fig. 5 for proposed structures).

In order to further predict some details of the adsorption mode of pyraclostrobin on the TiO$_2$ surface, point charges of all individual atoms in pyraclostrobin molecule were calculated as it is explained in Section 2.6. Other studies of point charges for explaining pH effect have been reported in previous works [18,19].

Then, at acidic pH, interaction between TiOH$_2^+$ and pyraclostrobin would occur through one or more atoms with higher negative charge densities presented in Fig. 3. As it can be observed, negative charges were mainly localized on the nitrogen and the two oxygen atoms of the carbamate group [N (-0.297) and

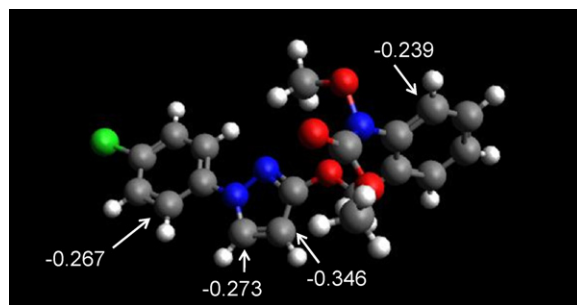**Fig. 5.** Photocatalytic degradation pathway of pyraclostrobin.

Fig. 7. Higher negative charge densities on C atoms in pyraclostrobin.

intermediates. Blank analysis helped us to discard those peaks coming from the sample handling procedure and chromatographic system.

First, molecular weights of photoproducts were determined by Full scan analysis in negative and/or positive acquisition mode. Then, MS/MS of the major compound were performed in order to obtain structural information of each photoproduct. Fig. 4 shows the single ion monitoring (SIM) trace in positive ionization of the pyraclostrobin and the 11 major intermediates detected and subsequently identified by interpretation of their MS spectra. These compounds are summarized in Table 2 together with their LC–MS retention times, molecular weights, fragments and structure.

Based on the results and on the densities charges, a possible photocatalytic degradation pathway of pyraclostrobin consisting of several steps was proposed in Fig. 5. As can be seen, all the intermediates are formed in mainly three different ways:

(a) In the first case, pyraclostrobin was attacked by OH• radicals in the chlorophenyl and pyrazol rings in left moiety of the pesticide molecule leading to three monohydroxylated products **2**, **4** and **5**, which reached their maximum of concentration around 20 min and decreased progressively to disappear from solution after 120 min, as showed in Fig. 6a.

   In order to determine the position of the −OH addition, pyraclostrobin mass fragmentation spectra were firstly compared to the photoproducts masses observed during product ion scan analysis. These compounds exhibited the same molecular fragment as pyraclostrobin ($m/z = 194$) which corresponds to the right moiety without hydroxylation. The OH• radicals prefer to attack in atoms with a high negative density charge. In this moiety of the molecule, it can be observed in Fig. 7 that there were three C atoms with a high negative density (a C atom showed a charge of −0.267 in the chlorophenyl ring and two C atoms with −0.273 and −0.346 in the pyrazol ring) which led to the formation of the three mainly compounds mentioned above (**2**, **4** and **5**). The others C atoms belonging to these two rings showed negative charges lower than −0.1 and positives charges. The loss of the N-methoxy group led to compounds **8** and **9** which were much more concentrated that the first ones.

(b) Compound **3** was obtained in the same way as compounds **2**, **4** and **5** by hydroxylation of the aromatic ring in the right moiety of the pyraclostrobin molecule. The position of the hydroxylation was confirmed by the fragment with $m/z = 210$ which corresponds to the right moiety with −OH in the benzene ring. The most probable position of a possible attack of the OH• radicals would be on the C atom that showed the higher negative charge in the benzene ring (−0.239; Fig. 7)

   Later, the loss of N-methoxy group led to compound **6** and **7**. As it happened in case (a), these compounds showed a

Fig. 6. (a) Evolution of the intermediate compounds during degradation of pyraclostrobin according to way (a) of Fig. 5. (b) Evolution belonging to compounds of way (b) of Fig. 5. (c) Evolution of the intermediates obtained by way (c) of Fig. 5.

(−C=O−; −0.585/CH₃O−; −0.515)], on the another two oxygen atoms of pyraclostrobin molecule [N-methoxy (−0.289) and yloxymethyl (−0.348)], on the nitrogen atom of the pyrazol ring (−0.609) and on the chloride, with a contribution smaller than the other atoms (−0.153). However, this last one and the oxygen atom of the carbamate group (−C=O−) are the regions showing more accessibility in pyraclostrobin for interactions with catalyst surface. Therefore, when TiO₂ surface is positively charged below pH pzc (≈6.25) an attractive force between the TiOH₂⁺ surface groups and the pyraclostrobin molecules is operable. By contrast, at alkaline pH, repulsion between surface and pyraclostrobin is much more marked if it is considered that both species are negatively charged, thus preventing interaction and delaying degradation.

3.3. Identification and evolution of the organic intermediates

A mixture of five solutions of pyraclostrobin (2.3 mg L⁻¹) irradiated for 15, 30, 60, 90 and 180 min and concentrated by SPE was analyzed by HPLC–MS/MS in order to characterize all the organic

higher concentration that initial compound **3** (Fig. 6b).The last intermediates consisted of the substitution of chloride for an —OH group (compound **10**) and the scission of the 4-hydroxyphenyl and pyrazol bond (N—C bond) leading to the formation of compound **11** (Fig. 6c; this compound could be also obtained directly from pyraclostrobin as it is shown in Fig. 5). The subsequent rupture of the —C—O— bond of pyrazol and the oxygen of the yloxymethyl group produced compound **12**, which could be also obtained from compounds **8** and **9**.

3.4. Identification and evolution of carboxylic acids
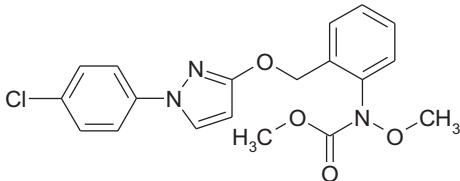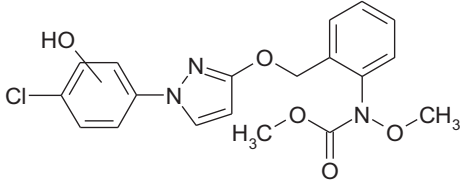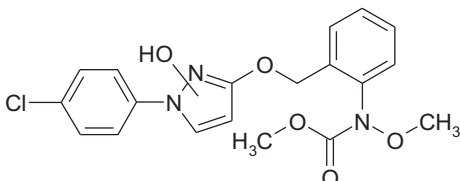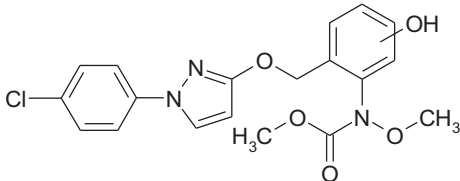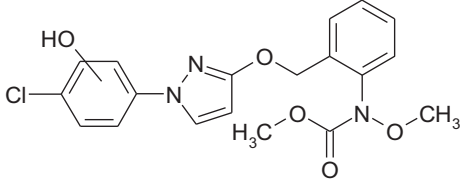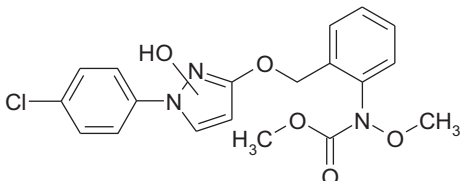
Four major carboxylic acids (oxalic, glyoxilic, malonic and acetic acids) formed during the degradation of the 5.9 μmol L^{-1}

of pyraclostrobin solution were identified by ion exchange chromatography by comparison of their retention time (t_R) with those of standards. They were formed since the beginning of irradiation and reached their maximum concentration after 30–45 min. Their kinetic evolution during the degradation of pyraclostrobin is represented in Fig. 8a.

Glyoxilic and malonic acids reached their maximum concentration of 7.2 and 18.1 μmol L^{-1}, respectively after 45 min of irradiation and then diminished progressively. Acetic acid reaches its maximum concentration after 30 min with a value of 15.8 μmol L^{-1}. However, oxalic acid is accumulated up to 5.4 μmol L^{-1} during 1 h and hence, it is slowly destroyed at 5 h. A tentative mechanism for the formation of carboxylic acids inferred from these data is showed in Fig. 8b.

Table 2
Mass spectra data and structures of identified intermediates by LC–MS for irradiation pyraclostrobin with TiO$_2$.

Structure	Peak n°	Retention time (min)	[M+H]	Fragment (Intensity)
	1	20.4	388	194.1 (100) 164.2 (45) 388.2$^{\#}$ (34) 296$^{\#}$ (25) 163.2 (18) 324.2 (7.3) 356$^{\#}$ 132$^{\#}$
or	2	20.1	404	194 (100) 164.1 (63) 162.9 (14) 179.1 (4)
	3	17.9	404	210 (100) 195 (20) 180 (15) 178.2 (15)
or	4	17.7	404	194.2 (100) 164 (32) 163.3 (16)

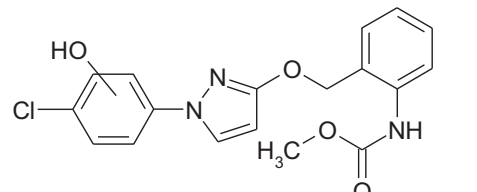$^{\#}$Fragments with chloride.

Table 2 (*Continued*)
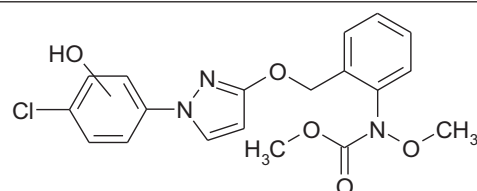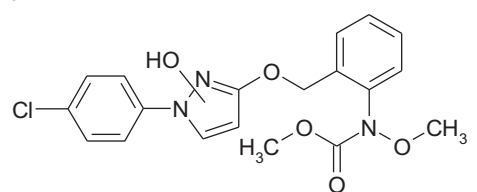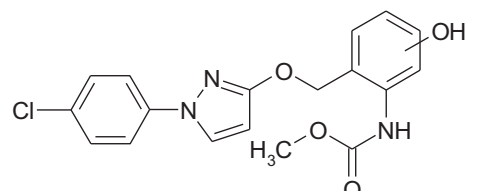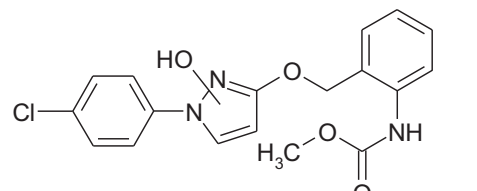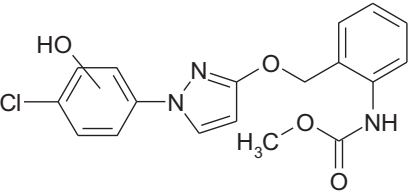
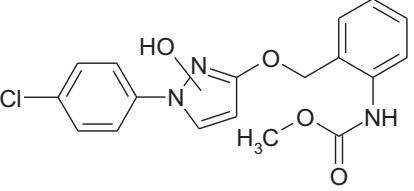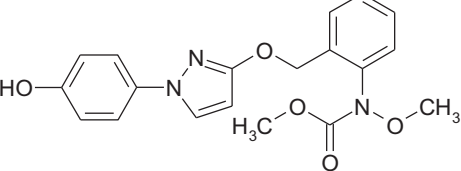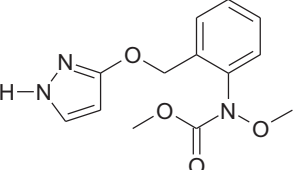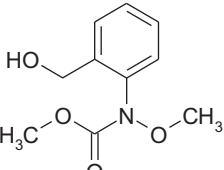|				
  or 	5	17.0	404	194 (100) 163.8 (30) 163.2 (10)
	6	17.7	374	180.1 (100) 148.2 (13) 195.3 (3) 342.1 (1)
	7	17.1	374	180.1 (100) 148.2 (29) 342.1 (11) 195.3 (2) 215.2 (1.5)
  Or 	8	13.4	374	194 (100) 164.2 (35) 163 (19) 134 (4) 132 (2)

Table 2 (*Continued*)

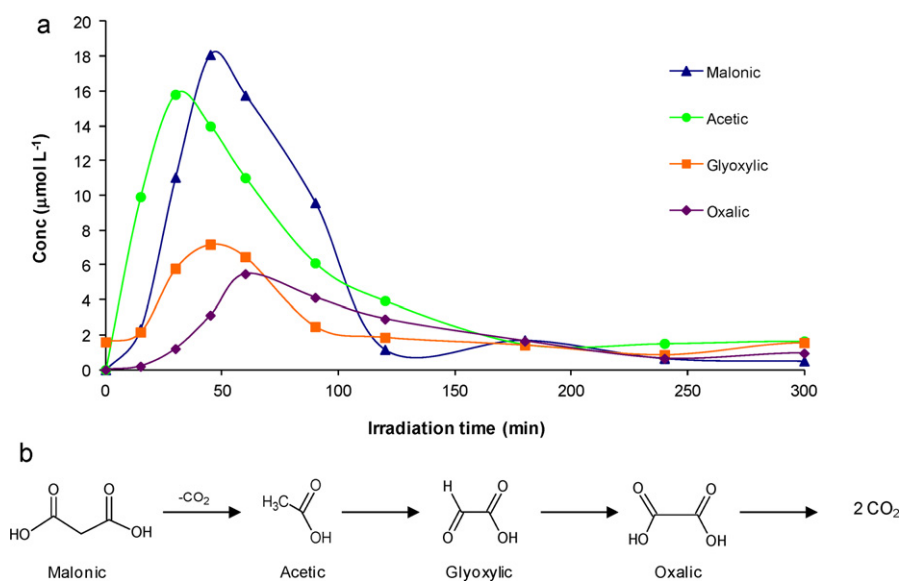| Structure				m/z
(structure: HO / Cl-phenyl pyrazole carbamate) Or (structure)	9	12.0	374	194 (100) 164.2 (37) 163 (23) 263.7 (7) 342.1 (6)
(structure: HO-phenyl pyrazole carbamate N–OCH₃)	10	15.7	370	194 (100) 164.2 (42) 163 (24) 278.2 (16) 338.4 (7) 306.1 (5)
(structure: H–N pyrazole carbamate N–O)	11	12.2	278	163.2 (100) 194.2 (100) 164 (73) 213.9 (48) 161.8 (27) 149.1 (17) 132.9 (13)
(structure: HO–CH₂-phenyl carbamate N–OCH₃)	12	8	212	194 (100) 163 (10) 133

Fig. 8. (a) Formation of carboxylic acids during pyraclostrobin photocatalytic degradation. (b) Proposed scheme for the formation of carboxylic acids.

4. Conclusions

Pyraclostrobin was totally degraded in an aqueous TiO$_2$ suspension in the dark after 60 min following a pseudo-first-order kinetic behavior. The rate constant for the reaction of pyraclostrobin was calculated as $k_{obs} = 1.4 \times 10^{-2}$ min^{-1}. The effect of pH on the rate constant value was studied in the range pH 2–10. The photodegradation rate was found to increase along with decreasing pH.

A careful study of the evolution of pyraclostrobin and the eleven intermediates monitored by HPLC-UV, and their identification using HPLC–APCI–MS/MS, allowed a better understanding of the mechanism of the degradation and a pathway of degradation has been tentatively proposed.

The main steps involve: hydroxylation of the aromatic rings (chloro-phenyl, phenyl and pyrazol) followed by the loss of the N-methoxy group, substitution of chloride atom by a hydroxyl group, rupture of the pyrazol and phenyl bond and the scission of the oxygen and pyrazol bond. Finally, oxidative degradation of pyraclostrobin by hydroxyl radicals leads to the formation of carboxylic acids such as oxalic, glyoxilic, malonic and acetic acids.

Acknowledgments

References

[1] A. Lair, C. Ferronato, J.M. Chovelon, J.M. Hermann, J. Photochem. Photobiol. A Chem. 193 (2008) 193–203.
[2] Vulliet, J.M. Chovelon, C. Guillard, J.M. Hermann, J. Photochem. Photobiol. A: Chem. 159 (2003) 71–79.
[3] M. Tamimi, S. Qourzal, A. Assabbane, J.M. Chovelon, C. Ferronato, Y. Ait-Ichou, Photochem. Photobiol. Sci. 5 (2006) 477–482.
[4] G.R.M. Echavia, F. Matzusawa, N. Negishi, Chemosphere 76 (2009) 595–600.
[5] I. Konstantinou, T.M. Sakellarides, V.A. Sakkas, T.A. Albanis, Environ. Sci. Technol. 35 (2001) 398–405.
[6] O. Carp, C.L. Huisman, A. Reller, Prog. Solid State Chem. 32 (2004) 33–177.
[7] C.G. Da Silva, J.L. Faria, J. Photochem. Photobiol. A: Chem. 155 (2003) 133–143.
[8] Daneshvar, D. Salari, A.R. Khataee, J. Photochem. Photobiol. A: Chem. 157 (2003) 111–116.
[9] A.L. Linsebigler, G. Lu, J.T. Yates, Chem. Rev. 95 (1995) 735–758.
[10] A. Menezes Filhoa, F. Neves dos Santos, P.A. de, P. Pereira, Microchem. J. 96 (2010) 139–145.
[11] U.C. Singh, P.A. Kollman, J. Comput. Chem. 5 (1984) 129–145.
[12] Gaussian 09, Revision A.1, M.J. Frisch et al. Gaussian, Inc., Wallingford CT, 2009.
[13] J.C. D'Oliveria, G. Al-Sayyed, P. Pichat, Environ. Sci. Technol. 24 (1990) 990–996.
[14] C.S. Rurchi, D.R. Ollis, J. Catal. 122 (1990) 178–192.
[15] J.M. Herrmann, Top. Catal. 34 (2005) 49–65.
[16] C. Kormann, D.W. Bahnemann, M.R. Hoffmann, Environ. Sci. Technol. 25 (1991) 494–500.
[17] S.A. Houas, H. Lachheb, M. Ksibi, E. Elaloui, C. Guillard, J. Herrmann, Appl. Catal. B 31 (2001) 145.
[18] C. Guillard, S. Horikoshi, N. Watanabe, H. Hidaka, P. Pichat, J. Photochem. Photobiol. A: Chem. 149 (2002) 155.
[19] S. Horikoshi, N. Serpone, S. Yoshizawa, J. Knowland, H. Hidaka, J. Photochem. Photobiol. A: Chem. 120 (1999) 63.